# Holographic Nucleons [1]

Ismail Zahed

*Department of Physics and Astronomy, SUNY Stony-Brook, NY 11794*

October 29, 2010

**Abstract**

Recent developments in holography have provided a new vista to the nucleon composition. A strongly coupled core nucleon tied with vector mesons emerge in line with the Cheshire cat principle. The cat is found to hide in the holographic direction. We discuss the one, two and many baryon problem in this context and point at the striking similarities between the holographic results and recent lattice simulations at strong coupling.

[1] To appear in *Festschrift for Gerry Brown*, Ed. Sabine Lee, World Scientific

# 1 Dedication

*This paper is dedicated to Gerry Brown who has been my mentor and colleague for the past three decades. I have met Gerry while in graduate school way back at MIT, in Feshbach's office on a sunny fall morning. After the meeting, Gerry asked me when I would graduate as he was prepared to hire me for the next three years. I did the following spring and have been with Gerry since then. Gerry is an outstanding scientist and humanist that has contributed immensely to our field. I thank him for his guidance and friendship, and wish him well for the years to come.*

# 2 Introduction

Back in the eighties, quark bag models were proposed as models for hadrons that capture the essentials of asymptotic freedom through weakly interacting quarks and gluons within a bag, and the tenets of nuclear physics through strongly interacting mesons at the boundary. The delineation or bag radius was considered as a fundamental and physically measurable scale that separates ultraviolet from infrared QCD. Two competing pictures emerged: The original MIT bag model with a large radius surrounded by a bare vacuum and the Stony-Brook bag model with a small radius surrounded by pions [1]. In fact, at low energy this delineation is unphysical as stated in the Cheshire cat principle [2]. Quantum effects and anomalies cause most of the charges (fermionic, axial, etc.) to leak making the bag boundary immaterial [3], much like the smile of the Cheshire cat in "Alice in wonderland" [4]. The Skyrme model typifies the extreme realization of the Cheshire cat principle whereby the immaterial bag radius is reduced to zero size [5].

The Skyrme model realizes QCD baryons as chiral solitons in the limit of large number of colors $N_c$. Recently, the same model was found to emerge from holographic QCD in the dual limit of large $N_c$ and strong coupling t'Hooft coupling $\lambda = g^2 N_c$ [6, 7]. In the holographic construction, the Skyrmion is the holonomy of a flavor instanton tied to Witten's vertex in bulk [8]. Baryon number at the boundary is dual to instanton number in bulk. Although the exact holographic dualities are only known for a restricted set of string theories in bulk with mostly conformal field theories at the boundary [9], we will assume that such a correspondence holds for holographic QCD which is not conformal.

The present paper review some aspects of the holographic baryons following recent work in [10]. It is dedicated to Gerry Brown. In section 3, we review the holographic baryon construction from a bulk instanton, and emphasize the emergence of the Cheshire cat principle.


Figure 1: Alice's Cheshire Cat.


Figure 2: The Cheshire Cat Principle.

In section 4 a top-down holographic model is briefly summarized and the bayonic current derived. In section 5, the 2-nucleon problem is discussed usingthe ADHM 2-instanton configuration. In section 6, cold and dense holographic matter is argued to be a crystal of instantons at low densities, and a crystal of dyons at higher densities. In section 7, we estimate the melting temperature of these crystals into liquids. Our conclusions are summarized in section 8.

# 3 The Skyrmion from the Instanton

In holographic QCD, a baryon is initially described as a flavor instanton in an $R^{1,3} \times R_Z$ dimensional space where the holographic direction $R_Z$ is warped by gravity. At large t'Hooft coupling $\lambda = g^2 N_c$, the instanton is forced by gravity to drop to the bottom of $R_Z$. Topological (Coulomb) repulsion causes the instanton to lump at a size $Z \approx 1/\sqrt{\lambda} \ll 1$. In this limit, the effects of the gravitational warping on the instanton can be neglected. Thus the

instanton SU(2) flavor configuration $\mathbb{A}_M$ and its supporting U(1) Coulomb potential $\widehat{\mathbb{A}}_M$ read

$$\widehat{\mathbb{A}}_0 = -\frac{1}{8\pi^2 a\lambda}\frac{2\rho^2+\xi^2}{(\rho^2+\xi^2)^2} \ , \qquad\qquad \mathbb{A}_M = \eta_{iMN}\frac{\sigma_i}{2}\frac{2x_N}{\xi^2+\rho^2} \ , \tag{1}$$

with all other gauge components zero. The size is $\rho \sim 1/\sqrt{\lambda}$. We refer to [6] (last reference) for more details on the relevance of this configuration for baryons. The ADHM configuration has maximal spherical symmetry and satisfies

$$(\mathbb{R}\mathbb{A})_Z = \mathbb{A}_Z(\mathbb{R}\vec{x}) \ , \qquad (\mathbb{R}^{ab}\mathbb{A}^b)_i = \mathbb{R}^T_{ij}\mathbb{A}^a_j(\mathbb{R}\vec{x}) \ , \tag{2}$$

with $\mathbb{R}^{ab}\tau^b = \Lambda^+\tau^a\Lambda$ a rigid SO(3) rotation, and $\Lambda$ is SU(2) analogue..

The holographic baryon is just the holonomy of (1) along the gravity bearing and conformal direction $Z$,

$$U^{\mathbb{R}}(x) = \Lambda\mathbf{P}\text{exp}\left(-i\int_{-\infty}^{+\infty} dZ\,\mathbb{A}_Z\right)\Lambda^+ \ . \tag{3}$$

The corresponding Skyrmion in large $N_c$ and leading order in the strong coupling $\lambda$ is $U(\vec{x}) = e^{i\vec{\tau}\cdot\vec{x}\mathbf{F}(\vec{x})}$ with the profile

$$\mathbf{F}(\vec{x}) = \frac{\pi|\vec{x}|}{\sqrt{\vec{x}^2+\rho^2}} \ . \tag{4}$$

The holonomy (33) is a heavy flavor but colorless fermion "propagating" along the holographic direction with the instanton as a background field. The result is a small size Skyrmion map $U(x)$ at the boundary.

The baryon emerges from a semiclassical organization of the quantum fluctuations around the point-like source (33). To achieve this, we define

$$A_M(t,x,Z) = \mathbb{R}(t)\left(\mathbb{A}_M(x-X_0(t),Z-Z_0(t)) + C_M(t,x-X_0(t),Z-Z_0(t))\right) \ , \tag{5}$$

The collective coordinates $\mathbb{R}, X_0, Z_0, \rho$ and the fluctuations $C$ in (5) form a redundant set.

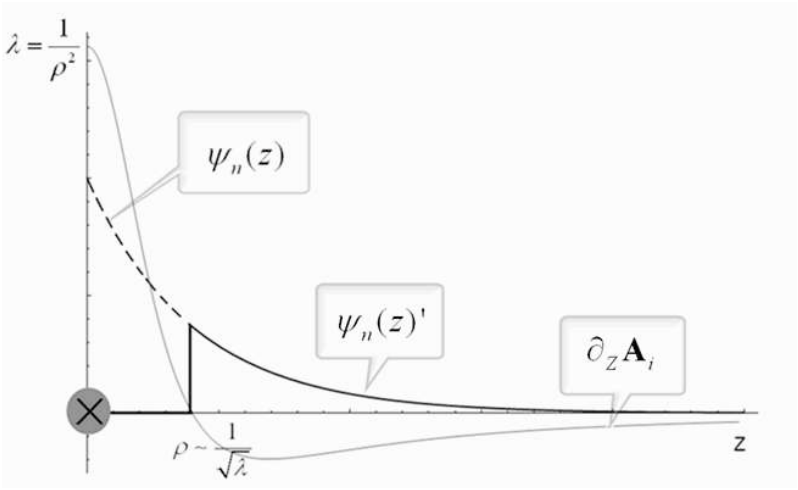


Figure 3: The Z-mode in the non-rigid gauge vs $\partial_Z \mathbb{A}_i$.

The redundancy is lifted by constraining the fluctuations to be orthogonal to the zero modes. This can be achieved either rigidly [11] or non-rigidly [12]. We choose the latter as it is causality friendly. For the collective iso-rotations the non-rigid constraint reads

$$\int_{x=Z=0} d\hat{\xi} C \, G^B \mathbb{A}_M \ , \tag{6}$$

with $(G^B)^{ab} = \epsilon^{aBb}$ the real generators of $\mathbb{R}$.

For $Z$ and $\rho$ the non-rigid constraints are more natural to implement since these modes are only soft near the origin at large $\lambda$. The vector fluctuations at the origin linearize through the modes

$$d^2\psi_n/dZ^2 = -\lambda_n \psi_n \ , \tag{7}$$

with $\psi_n(Z) \sim e^{-i\sqrt{\lambda_n}Z}$. In the spin-isospin 1 channel they are easily confused with $\partial_Z \mathbb{A}_i$ near the origin as we show in Fig. 3. Using the non-rigid constraint, the double counting is removed by removing the origin from the vector mode functions

$$\psi_n'(Z) = \theta(|Z| - Z_C)\psi_n(Z) \ , \tag{8}$$

with $Z_C \sim \rho \sim 1/\sqrt{\lambda}$ which becomes the origin for large $\lambda$. In the non-rigid semiclassical framework, the baryon at small $\xi < |Z_C|$ is described by a flat or uncurved instanton located at the origin of $R^4$ and rattling in the vicinity of $Z_C$. At large $\xi > |Z_C|$, the rattling

instanton sources the vector meson fields described by a semi-classical expansion with non-rigid Dirac constraints. Changes in $Z_C$ (the core boundary) are reabsorbed by a residual gauge transformation on the core instanton. This is a holographic realization of the Cheshire cat principle [2] where $Z_C$ plays the role of the Cheshire cat smile. In a way, Alice's Cheshire cat of Fig. 1 has gone out of sight in the holographic or 5th direction.

# 4 The Baryonic Current

To illustrate the Cheshire cat mechanism more quantitatively, we now summarize the holographic Yang-Mills-Chern-Simons action in 5D curved background. This is the leading term in a $1/\lambda$ expansion of the D-brane Born-Infeld (DBI) action on D8 [6],

$$S = S_{YM} + S_{CS} \ , \tag{9}$$

$$S_{YM} = -\kappa \int d^4x dZ \ \mathrm{tr} \left[ \frac{1}{2} K^{-1/3} \mathcal{F}_{\mu\nu}^2 + M_{\mathrm{KK}}^2 K \mathcal{F}_{\mu Z}^2 \right] \ , \tag{10}$$

$$S_{CS} = \frac{N_c}{24\pi^2} \int_{M^4 \times R} \omega_5^{U(N_f)}(\mathcal{A}) \ , \tag{11}$$

where $\mu, \nu = 0, 1, 2, 3$ are 4D indices and the fifth(internal) coordinate $Z$ is dimensionless. There are three things which are inherited by the holographic dual gravity theory: $M_{\mathrm{KK}}, \kappa$, and $K$. $M_{\mathrm{KK}}$ is the Kaluza-Klein scale and we will set $M_{\mathrm{KK}} = 1$ as our unit. $\kappa$ and $K$ are defined as

$$\kappa = \lambda N_c \frac{1}{216\pi^3} \equiv \lambda N_c a \ , \qquad K = 1 + Z^2 \ . \tag{12}$$

$\mathcal{A}$ is the 5D $U(N_f)$ 1-form gauge field and $\mathcal{F}_{\mu\nu}$ and $\mathcal{F}_{\mu Z}$ are the components of the 2-form field strength $\mathcal{F} = \mathrm{d}\mathcal{A} - i\mathcal{A} \wedge \mathcal{A}$. $\omega_5^{U(N_f)}(\mathcal{A})$ is the Chern-Simons 5-form for the $U(N_f)$ gauge field

$$\omega_5^{U(N_f)}(\mathcal{A}) = \mathrm{tr} \left( \mathcal{A}\mathcal{F}^2 + \frac{i}{2}\mathcal{A}^3\mathcal{F} - \frac{1}{10}\mathcal{A}^5 \right) \ , \tag{13}$$

We note that $S_{YM}$ is of order $\lambda$, while $S_{CS}$ is of order $\lambda^0$. These terms are sufficient to carry a semiclassical expansion around the holonomy (33) with $\hbar = 1/\kappa$ as we now illustrate it for the baryon current.

To extract the baryon current, we source the reduced action with $\hat{\mathcal{V}}_\mu(x)$ a $U(1)_V$ flavor

field on the boundary in the presence of the vector fluctuations ($C = \hat{v}$). The tree level baryonic current reads

$$\begin{aligned} J^{\mu}_{B}(x) &= -\kappa K\widehat{\mathbb{F}}^{Z\mu}(x,Z)\,(1-\sum_{n=1}^{\infty}\alpha_{v^n}\psi_{2n-1})\Big|_{Z=B} \\ &\quad -\sum_{n,m}\; m^2_{v^n}a_{v^n}\psi_{2m-1}\int d^4y\;\kappa K\widehat{\mathbb{F}}_{Z\nu}(y,Z)\Delta^{\nu\mu}_{mn}(y-x)\Big|_{Z=B}\;. \end{aligned} \tag{14}$$

The massive vector meson propagator in Lorentz gauge is

$$\Delta^{mn}_{\mu\nu}(x) = \int \frac{d^4p}{(2\pi)^4}e^{-ipx}\left[\frac{-g_{\mu\nu}-p_\mu p_\nu/m^2_{v^n}}{p^2+m^2_{v^n}}\delta^{mn}\right]\;, \tag{15}$$

The first contribution in (14) is the direct coupling between the core instanton and the $U(1)_V$ source as displayed in Fig. 2a. The second contribution sums up the omega, omega', ... contributions as displayed in Fig. 2b. We note that the direct or core coupling drops by the exact sum rule

$$\sum_{n=1}^{\infty}\alpha_{v^n}\psi_{2n-1} = 1\;, \tag{16}$$

following from closure in curved space

$$\delta(Z-Z') = \sum_{n=1}^{\infty}\;\kappa\psi_{2n-1}(Z)\psi_{2n-1}(Z')K^{-1/3}(Z')\;. \tag{17}$$

after integrating over the tower of omega meson trajectory. Vector Meson Dominance (VMD) is exact in holography. A similar argument holds for the pion electromagnetic form factor in [6]. The results presented in this section were derived in [10] using the cheshire cat descriptive. They were independently arrived at in [13] using the strong coupling source quantization. They also support, the bottom up effective approach described in [14] using the heavy nucleon expansion.

For many years Gerry Brown has been advocating the 50/50 scenario for the baryon form factor using both phenomenology and his democratic principle. In many ways, the present unwinding of the baryon current in holography supports that. Indeed, if we were to truncate the resonance contributions to the lowests, say the omega, then the core contribution is non-zero. In this case, the deleniation of the Cheshire cat smile is no longer arbitrary. A specific

Figure 4: Gerry Brown 50/50 scenario: Direct (left) + VMD (right). See text.

position of the smile, will garentee optimal rearrangement between the truncated cloud and the core contributions, thereby vindicating Gerry's 50/50 scenario.

# 5 2-Skyrmions from 2-Instantons

The procedure from the 1-nucleon sector to the 2-nucleon sector in holography relies on substituting the 1-instanton by the 2-instanton configuration. The latter is encoded in the ADHM data $\Delta$ which is a $(1+k)\times k$ matrix [15, 16]

$$\Delta = \begin{pmatrix} \lambda_1 & \lambda_2 \\ D-x & u \\ u & -D-x \end{pmatrix} , \qquad \Delta^\dagger \equiv \begin{pmatrix} \lambda_1^\dagger & (D-x)^\dagger & u^\dagger \\ \lambda_2^\dagger & u^\dagger & (-D-x)^\dagger \end{pmatrix} , \tag{18}$$

where the coordinates $x_M$ are defined as $x = x_M \sigma^M$, and the moduli parameters are encoded in the free parameters $\lambda_1, \lambda_2, D$: $|\lambda_i| \equiv \rho_i$ are the size parameters, $\lambda_1^\dagger \lambda_2/(\rho_1\rho_2) \in SU(2)$ is the relative gauge orientation, and $\pm D$ is the location of the constituents. $u$ is a parameter fixed by the ADHM constraint $\Delta^\dagger\Delta = f^{-1} \otimes \mathbf{1}$,

$$f^{-1} = \begin{pmatrix} \rho_1^2 + (x_M - D_M)^2 + \frac{\rho_1^2\rho_2^2 - (\lambda_1\cdot\lambda_2)^2}{4D_M^2} & \lambda_1\cdot\lambda_2 + 2x\cdot u \\ \lambda_1\cdot\lambda_2 + 2x\cdot u & \rho_2^2 + (x_M + D_M)^2 + \frac{\rho_1^2\rho_2^2 - (\lambda_1\cdot\lambda_2)^2}{4D_M^2} \end{pmatrix} , \tag{19}$$

where the notation $q\cdot p$ for two quaternions $q$ and $p$ is used,

$$q\cdot p \equiv \sum_M q_M p_M \ . \tag{20}$$

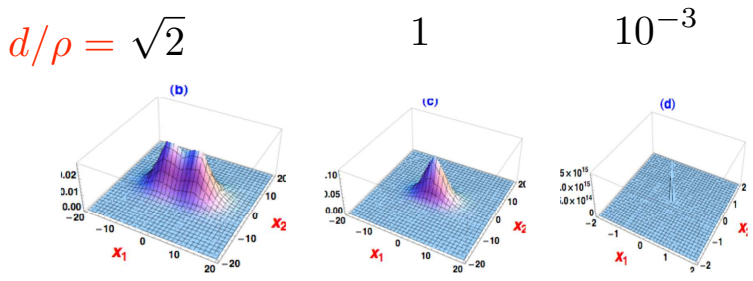


Figure 5: 2-Skyrmions from 2-Instantons: Defensive

$\rho_i = \sqrt{\lambda_i \cdot \lambda_i}$ are the size parameters, $\pm D_M$ the relative positions of the instantons, and

$$2x \cdot u = \frac{1}{D \cdot D}\left[(\lambda_2 \cdot D)(\lambda_1 \cdot x) - (\lambda_1 \cdot D)(\lambda_2 \cdot x) - \epsilon^{MNPQ}(\lambda_2)_M(\lambda_1)_N D_P x_Q\right] \ . \tag{21}$$

Without loss of generality, we may choose the moduli parameters to be

$$\lambda_1 = \rho_1\,(0,0,0,1) \ , \quad \lambda_2 = \rho_2\left(\widehat{\theta}_a \sin|\,\theta|\,, \cos|\,\theta|\right) \ , \quad D = \left(\frac{d}{2}, 0, 0, 0\right) \ , \tag{22}$$

with $a = 1,2,3$, $|\,\theta| \equiv \sqrt{(\theta_1)^2 + (\theta_2)^2 + (\theta_3)^2}$ and $\widehat{\theta}_a \equiv \frac{\theta_a}{|\theta|}$. The spatial $x^1$ axis is chosen as the separation axis of two instantons at large distance $d$. The flavor orientation angles $(\theta_a)$ are relative to the $\lambda_1$ orientation. We assign an $SU(2)$ matrix $U$ to the relative angle orientations in flavor space

$$U \equiv \frac{\lambda_1^\dagger \lambda_2}{\rho_1 \rho_2} = e^{i\theta_a \tau^a} \in SU(2) \ . \tag{23}$$

which is associated with the orthogonal $SO(3)$ rotation matrix $R$ as

$$\begin{aligned} R_{ab} &= \frac{1}{2}\mathrm{tr}\,\left(\tau_a U \tau_b U^\dagger\right) \\ &= \delta_{ab}\cos 2|\,\theta| + 2\widehat{\theta}_a\widehat{\theta}_b \sin^2|\,\theta| + \epsilon_{abc}\widehat{\theta}_c \sin 2|\,\theta| \ . \end{aligned} \tag{24}$$

For instance $R_{ab}$ reads

$$\begin{pmatrix} \cos 2\theta_3 & \sin 2\theta_3 & 0 \\ -\sin 2\theta_3 & \cos 2\theta_3 & 0 \\ 0 & 0 & 1 \end{pmatrix} \ , \qquad \begin{pmatrix} 1 & 0 & 0 \\ 0 & \cos 2\theta_1 & \sin 2\theta_1 \\ 0 & -\sin 2\theta_1 & \cos 2\theta_1 \end{pmatrix} \ , \tag{25}$$

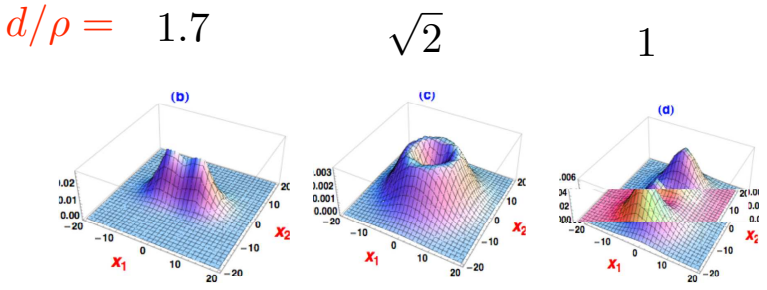


Figure 6: 2-Skyrmions from 2-Instantons: Combed

for $\theta_1 = \theta_2 = 0$ and $\theta_2 = \theta_3 = 0$ respectively. Note the double covering in going from SU(2) to SO(3).

In Fig. 5 we show the behavior of $\mathrm{Tr}(F_{\mu\nu}^2)$ for two parallell or defensive Skyrmions with $|\theta| = 0$ and $z = x_3 = 0$ and equal size cores $\rho = 9.64$ for several separations $d/\rho$. We recall that the physical core size in units of the KK-scale $M_K$ is $\rho M_K \equiv \rho M_K/\sqrt{\lambda}$. In Fig. 6 we show the behavior for two antiparallel or combed Skyrmions with $\theta_1 = \theta_2 = 0$ and $\theta_3 = \frac{\pi}{2}$ or $|\,\theta| = \pi/2$. This is a $\pi$ rotation along $x_3$ in the SO(3) notation (24). For large separation two lumps form along the $x^1$ axis. For smaller separation the two lumps are seen to form in the orthogonal or $x_2$ direction. In between a hollow baryon 2 configuration is seen which is the precursor of the donut seen in the baryon number 2 sector of the Skyrme model [17]. The concept of $\widetilde{d}$ as a separation at small separations is no longer physical given the separation taking place in the transverse direction. What is physical is the dual distance $u$ in the transverse plane.

At large separation, the nucleon-nucleon core interaction can be readily extracted from the Skyrmion-Skyrmion core interaction as it is linear in the $SO(3)$ rotation $R$. Indeed, the NN-potential can be decomposed as [18].

$$V_{NN} = V_1^+ + \vec{\tau}_1 \cdot \vec{\tau}_2\, V_1^- + \vec{\sigma_1} \cdot \vec{\sigma_2}\, \left(V_S^+ + \vec{\tau}_1 \cdot \vec{\tau}_2\, V_S^-\right) \tag{26}$$

$$+ \left(3(\vec{\sigma}_1 \cdot \widehat{d})(\vec{\sigma}_2 \cdot \widehat{d}) - \vec{\sigma}_1 \cdot \vec{\sigma}_2\right) \left(V_T^+ + \vec{\tau}_1 \cdot \vec{\tau}_2\, V_T^-\right) \tag{27}$$

with the core contribution

$$V_{1,\mathrm{core}}^+ \approx \frac{27\pi N_c}{2\lambda} \frac{1}{d^2}\,, \tag{28}$$

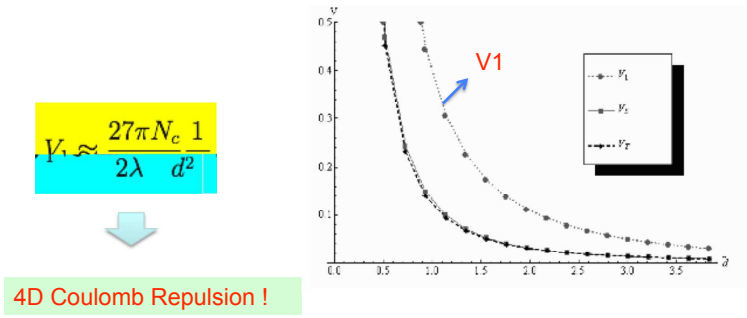


Figure 7: The central potential: Core contribution.

as shown in Fig. 7. This repulsion is Coulomb-like in 5-dimensions, a hallmark of holography. The cloud contributions are meson-mediated. To lowest order they read [18]

$$V^+_{1,\widehat{V}} \approx \sum_n G^2_{1\widehat{V},2n-1}\frac{e^{-m_{2n-1}d}}{4\pi\, d}\ , \qquad G_{1\widehat{V},2n-1} \equiv \frac{N_c}{2}\psi_{2n-1} \ \sim\ \sqrt{\frac{N_c}{\lambda}}\ , \tag{29}$$

$$V^-_{S,A} \approx \sum_n G^2_{SA,2n}\frac{e^{-m_{2n}d}}{4\pi d}\ , \qquad G_{SA,2n} \equiv -\frac{g_A\psi_{2n}}{\sqrt{6}\psi_0} \ \sim\ \sqrt{\frac{N_c}{\lambda}}\ , \tag{30}$$

$$V^-_{T,A} \approx \sum_n G^2_{TA,2n}\frac{e^{-m_{2n}d}}{4\pi d}\ , \qquad G_{TA,2n} \equiv \frac{g_A\psi_{2n}}{\sqrt{12}\psi_0} \ \sim\ \sqrt{\frac{N_c}{\lambda}}\ , \tag{31}$$

$$V^-_{T,\Pi} \approx \frac{1}{16\pi}\left(\frac{g_A}{f_\pi}\right)^2\frac{1}{d^3} \ \sim\ \frac{N_c}{\lambda}\ . \tag{32}$$

To order $N_c/\lambda$ we note $V^-_1 = V^+_S = V^+_T = 0$.

The present description of the 1- and 2-baryon configurations resemble in many ways the 1- and 2-nucleon structure emerging from strong coupling lattice QCD at finite density [19].

# 6 Dyonic Salt

At finite density, baryons crystalize at large $N_c$ irrespective of the 't Hooft coupling $\lambda$ since the Coulomb-like ratio is $\Gamma \approx N_c^2 \gg 1$. The crystal translates to a crystal of instantons in $T^3 \times R_Z$ with $R_Z$ the holographic direction. Periodic directions are accompanied by twists or holonomies. Twisted instantons or instantons with holonomies are known to topologically split, if the twist or the holonomy are strong enough. An example is the KvLL instanton in

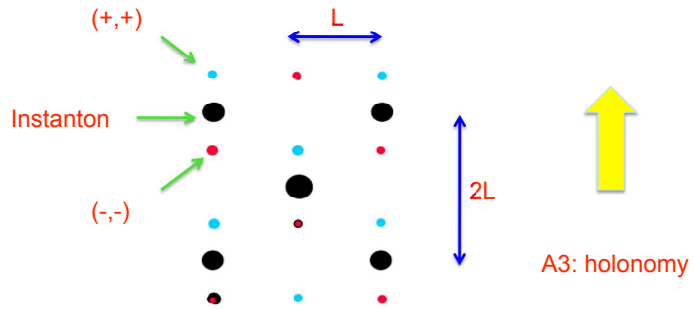


Figure 8: Instantons (black) Splitting into oppositely charged Dyons $(e, g) = (\pm, \pm)$.

$T^1 \times R^3$ [16, 20, 21] which is found to split into dyons.

Could such a splitting take place for an instanton arrangement in $T^3 \times R$? In [22] we suggested that it does, provided that the flavor gauge-symmetry is Higgsed, say the longitudinal "rho"

$$\langle \mathbf{A}_3^3 \rangle = \frac{2\pi}{2L} v\, T^3 \tag{33}$$

develops a non-vanishing expectation value. If that is the case, and proceeding by analogy with the KvLL instanton at finite temperature [16, 20, 21, 23], the periodic instanton array in space splits into a dyonic array. In Fig. 8 we show how an initial crystal arrangement of fcc dyons split into a crystal arrangement of bcc dyons under the action of the flavor holonomy [**?**]. The dyons are oppositely charged $e = g = \pm 1$ in units of $T^3$ along $x^3$. The dyon masses are $M_+ = MB_+ = Mv$ and $M_- = MB_- = M(1-v)$ – where $v$ is the Higgs vev – with $B_\pm$ their topological charges respectively [23]. We recall that $B_+ + B_- = v + (1-v) = 1$ is the instanton number. Here $2L$ is the cell size of the initial fcc instanton arrangement.

To order $N_c\lambda \approx \kappa$ the instantons and dyons are BPS with an arbitrary value of the vev $0 \leq v < 1$. The dyonic crystal is salt-like with intertwined lattices of topological charges $v$ and $(1-v)$ at the vertices. In Fig. 9 we display the fcc instanton crystal (left) as it splits to a bcc crystal of dyons under the action of the spatial holonomy along $x^3$.

The instantons cease to be BPS at next to next to leading order (NNLO). Indeed, at NNLO the core instantons repel at short distances as in (28). In general, the exact many-dyon interaction for all ranges is involved [20]. Fortunately, for our dyonic crystal the details of the dyonic interactions are not important in the non-BPS regime. Indeed, once the instantons split into $e = g = \pm 1$ dyons as in Fig. 8, the Coulomb nature of the underlying charges will

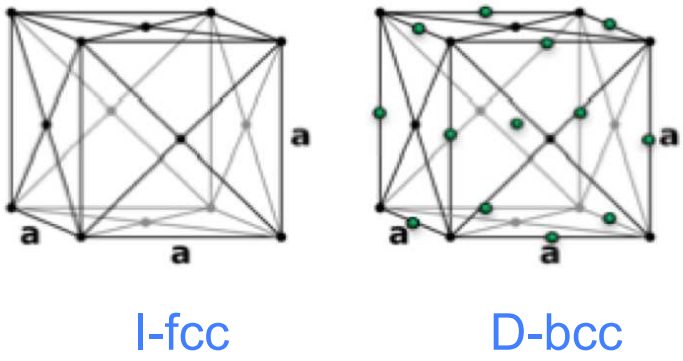


Figure 9: (a) Instantons in fcc; (b) Dyons in bcc.

cause them to arrange in a salt-like configuration to maximally screen the + and − charges, and therefore balance the Coulomb forces. The Coulomb balance leaves the vev $v$ arbitrary. However, the topological repulsion (28) wil maintain the Coulomb balance if $v = (1 - v)$. Thus $v = 1/2$ resulting into dyons of equal masses $M/2$ and equal charges $e = g = \pm 1$. This assumption is supported by dynamical calculations using colored instantons in SYM [24] and colored and thermal instantons in QCD in [25, 26].

The split dyon crystal arrangement is again salt-like with a unit cell $2L$ . This is a bcc crystal of half-instantons or dyons per cubic cell $L$. The instanton or baryon density is

$$n_B = \frac{1/2}{L^3} = \frac{4}{(2L)^3} \tag{34}$$

which is commensurate with the initial density of fcc instantons, namely a cell unit of $(2L)$ with 4 instantons. Hence our initial choice of the fcc configuration for the instantons at low density. (34) reflects on the half-instanton symmetry of the bcc dyonic salt, which is dual to the half-skyrmion symmetry on the boundary. The density at which the splitting takes place can be estimated using the KvLL instanton. Indeed, in the latter dyon separation $R_{+,-}$ is [16]

$$R_{+-} = 2\pi \frac{\rho^2}{2L} \tag{35}$$

with $\rho$ the KvLL instanton size with zero holonomy. Using (35) for our fcc crystal of cell size $(2L)^3$ and setting $R_{+-} = L$ at the transition to the bcc, yields $L = \sqrt{\pi}\rho$ or a critical density $n = 1/2/(\sqrt{\pi}\rho)^3$. In hQCD, $\rho \approx \sqrt{2/5}$ fm and $L \approx 1$ fm [22]. So the fcc to bcc transition

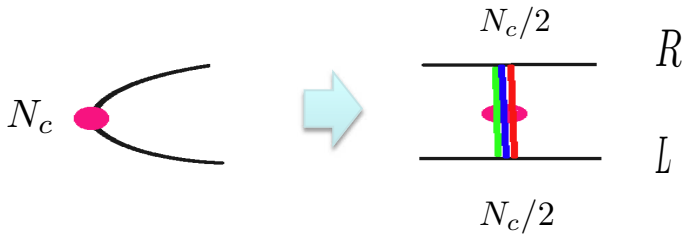


Figure 10: Geometrical reorganization of Witten's vertex from fcc (left) to (bcc) right.

takes place at $n_B \approx 1/2\,\mathrm{fm}^{-3}$ or 3 times nuclear matter density.

The energy density for which the fcc to bcc transition occurs can be estimated using only the Coulomb crystal (ignoring the core repulsion and the meson exchange attraction). The energy per baryon $E/N = M - \Delta$ is then [22]

$$\Delta = (e^2 + g^2)\,(T_3)^2\,\frac{\pi}{L}\,M_D \tag{36}$$

in the limit $\rho/L \ll 1$. $\Delta$ is the energy to bring a dyon in a bcc configuration and $M_D \approx 1.75$ is Madelung constant for salt [**?**]. For $L \approx 1$fm, $\Delta \approx 350$MeV. This estimate is on the high side since the Madelung constant for our 4-dimensional salt is smaller than that for the 3-dimensional salt, and $\rho/L \approx 1/\sqrt{\pi}$.

Does the dyonic salt configuration in bulk correspond to a chirally restored phase at high density? In [22] we have suggested that the Witten vertex maybe re-organized from the fcc to bcc configuration as shown in Fig. 10. In bulk, the probe flavor branes $D8 + \overline{D8}$ (left) split into separate $D8$ and $\overline{D8}$, each of which supporting its own crystal of 1/2-instantons or dyons ($L, R$ crystals). As a result, the right and left Wilson lines decouple

$$U^R_{1/2}(x) = P\exp\left(i\int_0^{+\infty}\mathbf{A}_Z(x,Z)\,dZ\right), \qquad U^L_{1/2}(x) = P\exp\left(i\int_{-\infty}^{0}\mathbf{A}_Z(x,Z)\,dZ\right) \tag{37}$$

The $L, R$ crystalline structures are commensurate with the $e = g = \pm 1$ dyonic structures as both are interchangeable by parity.

# 7 Dyonic Liquid

The cold dyonic crystal discussed in the preceding section can be dissociated by quanum fluctuations and/or thermal effects, both of which are subleading in the holographic counting. This notwithstanding, we may qualitatively ask how much temperature will be necessary to

melt the instanton or dyon crystals. For that, Lindemann criterion tells us that when the vibration amplitude of the lattice ion reaches 10% of the nearest neighbor distance $a_{NN}$, the classical lattice melts [28]

$$\sqrt{\langle x^2 \rangle} \approx 10\%\, a_{NN} \tag{38}$$

The mean-square vibration can be estimated from the Einstein formulae

$$M\omega_E^2 \left\langle x^2 \right\rangle = k_B T \tag{39}$$

with $\omega_E \approx c_S k_{\max} = c_S \pi / a_{NN}$ the Einstein frequency. The speed of sound $c_S$ in the crystal is related to its bulk compressibility $\mathbf{K}$,

$$\frac{c_S^2}{c^2} = \frac{\mathbf{K}}{n\, Mc^2} \approx (0.2 - 0.3)\, \frac{n_{NM}}{n} \tag{40}$$

with $n_{NM}$ again the nuclear matter density and $n$ the crystal baryon density. The last estimate borrows the typical nuclear matter compressibility estimate $\mathbf{K}/n_{NM} \approx 200 - 300\,\mathrm{MeV}$ [29]. Inserting (39) and (40) in the Lindemann criterion (38) yields the estimated melting temperature

$$\frac{k_B T}{Mc^2} \approx \pi^2\ (10\%)^2\ (0.2 - 0.3)\ \frac{n_{NM}}{n} \tag{41}$$

The higher the crystal density, the easier to melt by this estimate. We show in Fig. 11 a typical structure of the phase diagram at low temperature and large $N_c$. The fcc crystals melts to a Skyrmion liquid at about 30 MeV, while the dyonic salt melts into a dyonic liquid at about 10 MeV. The low nature of these melting temperatures is an early indication that these crystals are easily dissociated by quantum vibrations due to kinetic energy for instance.

# 8 Conclusions

In hQCD baryons emerge as holograms of instantons in a curved five-dimensional space. The baryons embody the essentials of the Cheshire cat principle, with the Cheshire cat found "hiding" in the holographic direction. A baryon with a small core and a rich cloud of vector mesons is unravelled. Exact vector dominance emerges when the entire Regge trajectory of the vectors is kept in the cloud.

The two-baryon configuration is naturally obtained from the two-instanton configuration in bulk using the ADHM construction. Many features of the Skyrmion-Skyrmion interactions

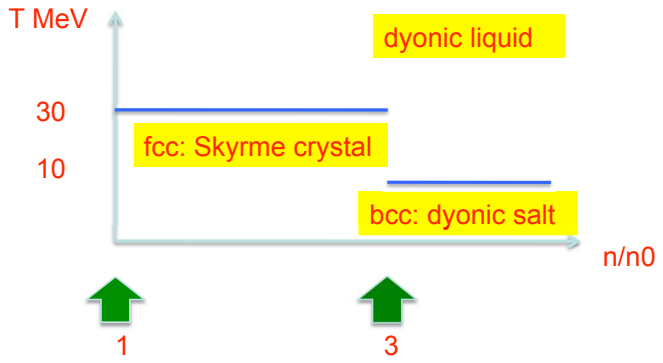


Figure 11: Phase diagram at large $N_c$ and low temperature.

are this way recovered. The adventage of hQCD over the Skyrme model is the fact that the boundary action for the baryons is entirely fixed by the gauge-gravity in bulk using the large $N_c$ and large $\lambda$ bookeeping.

Cold dense nucleonic systems crystallize at large $N_c$. The crystals are found to be an arrangement of instantons in the fcc configuration at low densities, and a bcc arrangement of dyons at higher densities. The transition occurs at about 3 times nuclear matter densities in hQCD. Quantum kinetic effects or thermal effects are likely to turn each of the crystal into a strongly interacting liquid of instantons for the former and dyons for the latter.

# 9 Acknowledgments

I thank K.Y. Kim, M. Rho and S.J. Sin for the many discussions during our long term collaboration on the issues discussed here. This work was supported in part by US-DOE grants DE-FG02-88ER40388 and DE-FG03-97ER4014.

# References

[1] A. Chodos, R. Jaffe, K. Johnson and C. Thorn, "Baryon structure in the bag theory", Phys. Rev. D **10**, 2599 (1974);
G.E. Brown and M. Rho, "The little bag," Phys. Lett. B **82**, 177 (1979).

[2] S. Nadkarni, H. B. Nielsen and I. Zahed, "Bosonization relations as bag boundary conditions," Nucl. Phys. B **253**, 308 (1985).

[3] H.B. Nielsen, M. Rho, A. Wirzba and I. Zahed, "Color anomaly in hybrid bag model," Phys. Lett. B **269**, 389 (1991);
M. Rho, "The Cheshire cat hadrons revisited," Phys. Rep. **240**, 1 (1994).

[4] L. Caroll, "Alice in Wonderland" Ed.

[5] I. Zahed and G.E. Brown, "The Skyrme model", Phys. Rep. **142**, 1 (19986).

[6] T. Sakai and S. Sugimoto, "Low energy hadron physics in holographic QCD," Prog. Theor. Phys. **113**, 843 (2005);
T. Sakai and S. Sugimoto, "More on a holographic dual of QCD," Prog. Theor. Phys. **114**, 1083 (2006);
H. Hata, T. Sakai, S. Sugimoto and S. Yamato, "Baryons from instantons in holographic QCD," arXiv:hep-th/0701280.

[7] D. Hong, M. Rho, H. Yee and P. Yi, "Chiral dynamics of baryons from string theory" Phys. Rev. bf D76, 061901 (2007).

[8] E. Witten, "Baryons and branes in anti de Sitter space", JHEP07, 006 (1998).

[9] J. Maldacena, "The large N limit of superconformal field theories and supergravity" Adv. Theor. Math. Phys. **2**, 231 (1998).

[10] K. Y. Kim and I. Zahed, "Electromagnetic baryon form factors from holographic QCD." JHEP **0809**, 007 (1998).

[11] C. Adami and I. Zahed, "Soliton quantization in chiral models with vector mesons," Phys. Lett. B **215** (1988) 387.

[12] H. Verschelde and H. Verbeke, "Nonrigid quantization of the skyrmion," Nucl. Phys. A **495** (1989) 523.

[13] K. Hashimoto, T. Sakai and S. Sugimoto, "Holographic baryons : static properties and form factors from gauge/string duality," arXiv:0806.3122 [hep-th].

[14] D. K. Hong, M. Rho, H. U. Yee and P. Yi, "Nucleon form factors and hidden symmetry in holographic QCD," arXiv:0710.4615 [hep-ph];

M. Rho, "Baryons and vector dominance in holographic dual QCD," arXiv:0805.3342 [hep-ph].

[15] M. F. Atiyah, N. J. Hitchin, V. G. Drinfeld and Yu. I. Manin, "Construction of instantons," Phys. Lett. A **65** (1978) 185.

[16] T. C. Kraan and P. van Baal, "Periodic instantons with non-trivial holonomy," Nucl. Phys. B **533**, 627 (1998) [arXiv:hep-th/9805168];

[17] E. Braaten and L. Carson, "The deuteron as a toroidal Skyrmion", Phys. Rev. bf D38, 3525 (1988)

[18] K. Y. Kim and I. Zahed, "Nucleon-nucleon potential from holography," JHEP **0903**, 131 (2009) [arXiv:0901.0012 [hep-th]];

[19] P. de Forcrand and M. Fromm, in talk "Nuclear Matter from strong coupling lattice QCD", Trento, July 2010; [arXiv:0907.1915], [arXiv:0912.2524].

[20] K. M. Lee and P. Yi, "Monopoles and instantons on partially compactified D-branes," Phys. Rev. D **56**, 3711 (1997) [arXiv:hep-th/9702107].

[21] K. M. Lee and C. h. Lu, "SU(2) calorons and magnetic monopoles," Phys. Rev. D **58**, 025011 (1998) [arXiv:hep-th/9802108].

[22] M. Rho, S.J. Sin and I. Zahed, "Dense QCD: A holographic dyonic salt", Phys. Let. **B689**, 23 (2010).

[23] D. Diakonov, "Topology and confinement," arXiv:0906.2456 [hep-ph].

[24] N. M .Davies, T. J. Hollowood, V. V. Khoze and M. P. Mattis, "Gluino condensate and magnetic monopoles in supersymmetric gluodynamics," Nucl. Phys. B **559**, 123 (1999) [arXiv:hep-th/9905015];

[25] A. R. Zhitnitsky, "Confinement-deconfinement phase transition in hot and dense QCD at large $N_c$," Nucl. Phys. A **813**, 279 (2008) [arXiv:0808.1447 [hep-ph]]; A. Parnachev and A. R. Zhitnitsky, "Phase Transitions, theta Behavior and Instantons in QCD and its Holographic Model," Phys. Rev. D **78**, 125002 (2008) [arXiv:0806.1736 [hep-ph]]; A. S. Gorsky, V. I. Zakharov and A. R. Zhitnitsky, "On Classification of QCD defects via holography," Phys. Rev. D **79**, 106003 (2009) [arXiv:0902.1842 [hep-ph]].

[26] M. N. Chernodub, A. D'Alessandro, M. D'Elia and V. I. Zakharov, "Thermal monopoles and selfdual dyons in the quark-gluon plasma," arXiv:0909.5441 [hep-ph].

[27] C. Kittel, *Introduction to solid state physics (8th ed.)* (John Wiley & Sons, 2005).

[28] P. Hofmann, *Solid state physics: an introduction.* (Wiley-VCH, 2008).

[29] J. P. Blaizot, Phys. Rep. **64**, 171 (1980).